ANALYSIS OF HIGH STEP-UP DC–DC CONVERTER OPERATION FOR PHOTOVOLTAIC MODULE APPLICATION

Vinoth kumar.P [1], Rekha.J [2]

Assistant professor [1], PG student [2]

Karpaga vinayaga college of engineering and technology[1, 2]

vino_pandiyan@yahoo.com [1], rekhapriya90@gmail.com [2]

Abstract—**Within the photovoltaic (PV) power-generation market, the ac PV module has shown obvious growth. However, a high voltage gain converter is essential for the module's grid connection through a dc–ac inverter. This paper proposes a converter that employs a floating active switch to isolate energy from the PV panel when the ac module is OFF; this particular design protects installers and users from electrical hazards. Without extreme duty ratios and the numerous turns-ratios of a coupled inductor, this converter achieves a high step-up voltage-conversion ratio; the leakage inductor energy of the coupled inductor is efficiently recycled to the load and mppt is used. These features explain the module's high-efficiency performance. The detailed operating principles and steady-state analyses of continuous and discontinuous conduction modes are described. A 15 V input voltage, 200 V output voltage, and 100 W output power prototype circuit of the proposed converter has been implemented; its maximum efficiency is up to 95.3% and full-load efficiency is 92.3% and simulated using MATLAB software.**

Index Terms—**AC module, coupled inductor, high step-up volt-age gain, single switch.**

I. INTRODUCTION

PHOTOVOLTAIC (PV) power-generation systems are becoming increasingly important and prevalent in distribution generation systems. A conventional centralized PV array is a serial connection of numerous panels to obtain higher dc-link voltage for main electricity through a dc–ac inverter [1], [30]. Unfortunately, once there is a partial shadow on some panels, the system's energy yield becomes significantly reduced [2]. An ac module is a micro inverter configured on the rear bezel of a PV panel [1]–[3]; this alternative solution not only immunizes against the yield loss by shadow effect, but also provides flexible installation options in accordance with the user's budget

[4]. Many prior research works have proposed a single-stage dc– ac inverter with fewer components to fit the dimensions of the bezel of the ac module, but their efficiency levels are lower than those of conventional PV inverters. However, employing a high step-up dc–dc converter in the front of the inverter improves power-conversion efficiency. When installing the PV generation system during daylight, for safety reasons, the ac module outputs zero voltage [4], [5]. Fig. 1 shows the solar energy through the PV panel and micro inverter to the output terminal when the switches are OFF.

When installation of the ac module is taking place, this potential difference could pose hazards to both the worker and the facilities. A floating active switch is designed to isolate the dc current from the PV panel, for when the ac module is off-grid as well as in the non operating condition. This isolation ensures the operation of the internal components without any residential energy being transferred to the output or input terminals, which could be unsafe.

The power capacity range of a single PV panel is about 100 W to 300 W, and the maxi-mum power point (MPP) voltage range is from 15 V to 40 V, which will be the input voltage of the ac module; in cases with lower input voltage, it is difficult for the ac module to reach high efficiency [3].
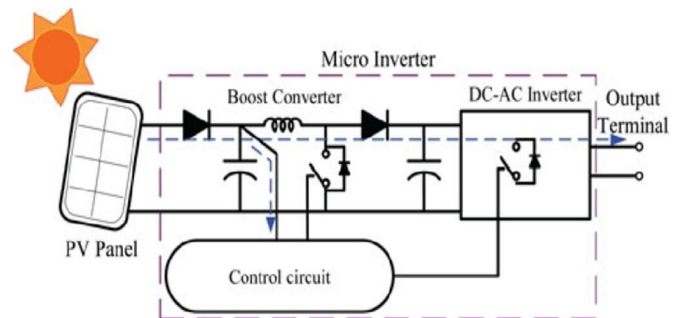

Fig.1. Potential difference on the output terminal of non floating switch micro inverter.

The micro inverter includes dc–dc boost converter, dc–ac inverter with control circuit as shown in Fig. 1. The dc–dc converter requires large step-up conversion from the panel's low voltage to the voltage level of the application. Previous research on various converters for high step-up applications has included analyses of the switched-inductor and switched-capacitor types [6], [7]; transformerless switched-capacitor type [8], [9], [29]; the voltage-lift type [12]; the capacitor-diode voltage multiplier [13]; and the boost type integrated with a coupled inductor [10], [11], these converters by increasing turns ratio of coupled inductor obtain higher voltage gain than conventional boost
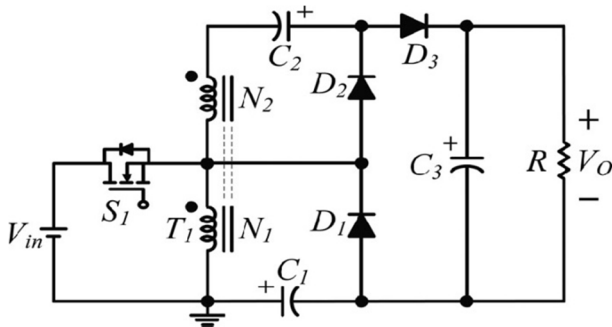

Fig. 2.   Circuit configuration of proposed converter.

or the reverse-recovery issue of the diodes. In addition, the equivalent series resistance (ESR) of the capacitor and the parasitic resistances of the inductor also affect overall efficiency. Use of active clamp technique not only recycles the leakage inductor's energy but also constrains the voltage stress across the active switch, how-ever the tradeoff is higher cost and complex control circuit [25], [26]. By combining active snubber, auxiliary resonant circuit, synchronous rectifiers, or switched- capacitor-based resonant circuits and so on, these techniques made active switch into zero voltage switching (ZVS) or zero current switching (ZCS) op-eration and improved converter efficiency [20]–[24]. However, when the leakage-inductor energy from the coupled inductor can be recycled, the voltage stress on the active switch is reduced, which means the coupled inductor employed in combination with the voltage-multiplier or voltage-lift technique success-fully accomplishes the goal of higher voltage gain [6]–[13].

The proposed converter, shown in Fig. 2, is comprised of a coupled inductor T_1 with the floating active switch S_1. The primary winding N_1 of a coupled inductor T_1 is similar to the input inductor of the conventional boost converter, and capacitor C_1 and diode D_1 receive leakage inductor energy from N_1. The secondary winding N_2 of coupled

converter. Some converters successfully combined boost and fly back converters, since various converter combinations are developed to carry out high step-up voltage gain by using the coupled-inductor technique [14]–[19], [27], [28]. The efficiency and voltage gain of the dc–dc boost converter are constrained by either the parasitic effect of the power switches
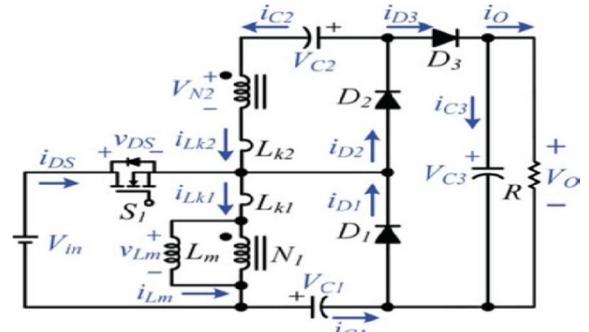
inductor T_1 is connected with another pair of capacitors C_2 and diode D_2, which are in series with N_1 in order to further enlarge the boost voltage. The rectifier diode D_3 connects to its output capacitor C_3. The proposed converter has several features: 1) The connection of the two pairs of inductors, capacitor, and diode gives a large step-up voltage-conversion ratio; 2) the leakage-inductor energy of the coupled inductor can be recycled, thus increasing the efficiency and restraining the voltage stress across the active switch; and 3) the floating active switch efficiently isolates the PV panel energy during nonoperating conditions, which enhances safety. The operating principles and steady-state analysis of the proposed converter are presented in the following sections.

II.   OPERATING PRINCIPLES OF THE PROPOSED CONVERTER

The simplified circuit model of the proposed converter is shown in Fig. 3. The coupled inductor T_1 is represented as a magnetizing inductor L_m, primary and secondary leakage in-ductors $L_{k\,1}$ and $L_{k\,2}$, and an ideal transformer. In order to sim-plify the circuit analysis of the proposed converter, the following assumptions are made.

The assumptions are list as following:

1) All components are ideal, except for the leakage induc-tance of coupled inductor T_1, which is being taken under consideration. The on-state resistance $R_{DS(ON)}$ and all parasitic capacitances of the main switch S_1 are neglected, as are the forward voltage drops of diodes $D_1 \sim D_3$.

2) The capacitors $C_1 \sim C_3$ are sufficiently large that the

voltages across them are considered to be constant.

3) The ESR of capacitors $C_1 \sim C_3$ and the parasitic resistance of coupled inductor T_1 are neglected.
4) The turns ratio n of the coupled inductor T_1 windings is equal to N_2 / N_1.

III MPPT Techniques

P&O Method

The Perturb and Observe (P&O) method is one of the most commonly used methods in practice. The P&O algorithms operate by periodically perturbing, i.e. incrementing or decrementing, the array terminal voltage and comparing the PV output power with that of the previous perturbation cycle. If the PV array operating voltage changes and power increases, the control system moves the PV array operating point in that direction. Otherwise the operating point is moved in the opposite direction.

The logic of this algorithm and the flowchart are explained in Fig. 4. The operating voltage of the PV system is perturbed by a small increment of $\Box V$, and this resulting change in $\Box P$. If $\Box P$ is positive, the perturbation of the operating voltage needs to be in the same direction of the increment. On the contrary, if $\Box P$ is negative, the obtained system operating point moves away from the MPPT and the operating voltage needs to move in the opposite direction of the increment.

A common shortcoming of this method is that the array terminal voltage is   perturbed every MPPT cycle. Therefore,
when the MPP is reached, the output power oscillates around the maximum, resulting in a power loss in the PV system.

Furthermore, it sometimes fails to find the MPP under the continuously increasing or decreasing irradiation conditions.

However, employing a high step-up dc–dc converter in the front of the inverter improves power-conversion efficiency.However, employing a high step-up dc–dc converter in either the parasitic effect of the power switches.
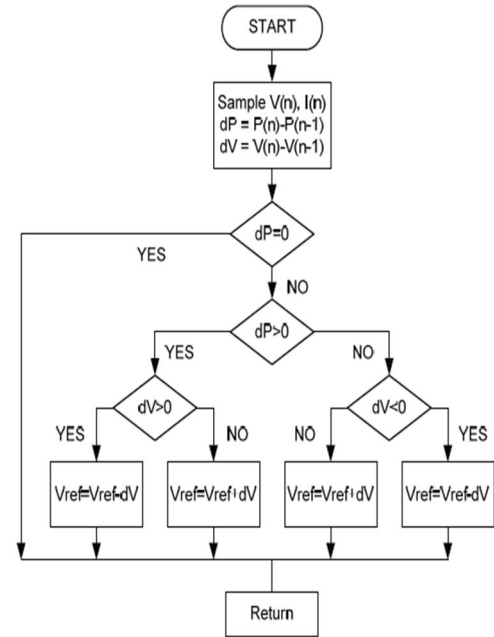

Fig 4. P&O method flowchart

The operating principle of continuous conduction mode (CCM) is presented in detail. The current waveforms of major components are given in Fig. 5. There are five operating modes in a switching period. The operating modes are described as follows

A. CCM Operation

Mode I [t_0 , t_1]: In this transition interval, the magnetizing in-ductor L_m continuously charges capacitor C_2 through T_1 when S_1 is turned ON. The current flow path is shown in Fig. 7(a); switch S_1 and diode D_2 are conducting. The current $i_{L\,m}$ is de-creasing because source voltage V_{in} crosses magnetizing induc-tor L_m and primary leakage inductor $L_{k\,1}$; magnetizing inductor L_m is still transferring its energy through coupled inductor T_1 to charge switched capacitor C_2 , but the energy is decreasing; the charging current $i_{D\,2}$ and $i_{C\,2}$ are decreasing. The secondary leakage inductor current $i_{L\,K\,2}$ is declining as equal to $i_{L\,m} / n$. Once the increasing $i_{L\,k\,1}$ equals decreasing $i_{L\,m}$ at $t = t_1$, this mode ends.

Mode II [t_1 , t_2]: During this interval, source energy V_{in} is series connected with N_2 , C_1 , and C_2 to charge output ca-pacitor C_3 and load R; meanwhile magnetizing inductor L_m is also receiving energy from V_{in} . The current flow path is shown in Fig. 7(b), where switch S_1 remains ON, and only diode D_3 is conducting. The $i_{L\,m}$, $i_{L\,k\,1}$, and $i_{D\,3}$ are

increasing because the V_{in} is crossing L_{k1}, L_m, and primary winding N_1; L_m and L_{k1} are storing energy from V_{in}; meanwhile V_{in} is also seri-ally connected with secondary winding N_2 of coupled inductor T_1, capacitors C_1, and C_2, and then discharges their

Fig. 5   Some typical waveforms of proposed converters at CCM   operation.

energy to capacitor C_3 and load R. The i_{in}, i_{D3} and discharging current $/i_{C1}/$ and $/i_{C2}/$ are increasing. This mode ends when switch S_1 is turned OFF at $t = t_2$.

Mode III [t_2, t_3]: During this transition interval, secondary leakage inductor L_{k2} keeps charging C_3 when switch S_1 is OFF. The current flow path is shown in Fig. 7(c), where only diode D_1 and D_3 are conducting. The energy stored in leakage inductor L_{k1} flows through diode

D_1 to charge capacitor C_1 instantly when S_1 is OFF. Meanwhile, the energy of secondary leakage inductor L_{k2} is series connected with C_2 to charge output capacitor C_3 and the load. Because leakage inductance L_{k1} and L_{K2} are far smaller than L_m, i_{Lk2} rapidly decreases, but i_{Lm} is increasing because magnetizing inductor L_m is receiving energy from L_{k1}. Current i_{Lk2} decreases until it reaches zero; this mode ends at $t = t_3$.
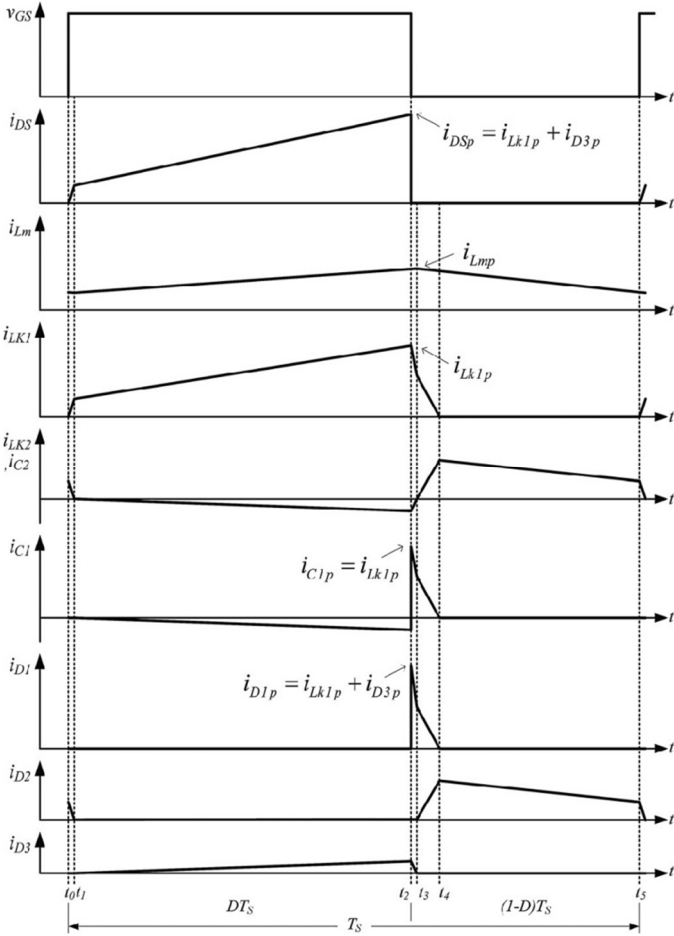
Mode IV [t_3, t_4]: During this transition interval, the energy stored in magnetizing inductor L_m is released to C_1 and C_2 simultaneously. The current flow path is shown in Fig. 7(d). Only diodes D_1 and D_2 are conducting. Currents i_{Lk1} and i_{D1} are continually decreased because the leakage energy still flowing through diode D_1 keeps charging capacitor C_1. The L_m is delivering its energy through T_1 and D_2 to charge capacitor C_2. The energy stored in capacitor C_3 is constantly.
discharged to the load R. These energy transfers result in decreases in i_{L1} and i_{Lm} but increases in i_{Lk2}. This mode ends when current i_{Lk1} is zero, at $t = t_4$.

Mode V [t_4, t_5]: During this interval, only magnetizing in-ductor L_m is constantly releasing its energy to C_2. The current flow path is shown in Fig. 7(e), in which only diode D_2 is con-ducting. The i_{Lm} is decreasing due to the magnetizing inductor energy flowing through the coupled inductor T_1 to secondary winding N_2, and D_2 continues to charge capacitor C_2. The en-ergy stored in capacitor C_3 is constantly discharged to the load R. This mode ends when switch S_1 is turned ON at the beginning of the next switching period.

B.   DCM Operation

The detailed operating principles for discontinuous-conduction-mode (DCM) operation are presented in this section. Fig. 6 depicts several typical waveforms during five operating modes of one switching period. The operating modes are de-scribed as follows.

Mode I [t_0, t_1]: During this interval, source energy V_{in} is series connected with N_2, C_1, and C_2 to charge output capacitor C_3 and load R; meanwhile, magnetizing inductor L_m is also receiving energy from V_{in}. The current flow path is shown in Fig. 8(a), which depicts that switch S_1 remains ON, and only diode D_3 is conducting. The i_{Lm}, i_{Lk1}, and i_{D3} are increasing because the V_{in} is crossing L_{k1}, L_m, and primary winding N_1; L_m and L_{k1} are storing energy from V_{in}; meanwhile, V_{in} also is serially connected with secondary winding N_2 of coupled inductor T_1, capacitors C_1, and C_2; then they all discharge their energy to

capacitor C_3 and load R. The i_{in} , $i_{D\,3}$ and discharging current $/i_{C\,1}/$ and $/i_{C\,2}/$ are increasing. This mode ends when switch S_1 is turned OFF at $t = t_1$.

Mode II $[t_1$, t_2]: During this transition interval, secondary leakage inductor $L_{k\,2}$ keeps charging C_3 when switch S_1 is OFF. The current flow path is shown in Fig. 8(b), and only diode D_2 and D_3 are conducting. The energy stored in leakage inductor $L_{k\,1}$ flows through diode D_1 to charge capacitor C_1 instantly when S_1 is OFF. Meanwhile, the energy of secondary leakage inductor $L_{k\,2}$ is series-connected with C_2 to charge output capacitor C_3 and the load. Because leakage inductance $L_{k\,1}$ and $L_{K\,2}$ are far smaller than L_m , $i_{L\,k\,2}$ decreases rapidly, but $i_{L\,m}$ is increasing because magnetizing inductor L_m is receiving energy from $L_{k\,1}$. Current $i_{L\,k\,2}$ reduces down to zero, and this mode ends at $t = t_2$.

Mode III $[t_2$, t_3]: During this transition interval, the energy stored in coupled inductor T_1 is releasing to C_1 and C_2 . The current flow path is shown in Fig. 8(c). Only diodes D_1 and D_2 are conducting. Currents $i_{L\,k\,1}$ and $i_{D\,1}$ are continually decreased because leakage energy still flowing through diode D_1 keeps charging capacitor C_1 . The L_m is delivering its energy through T_1 and D_2 to charge capacitor C_2 . The energy stored in capacitor C_3 is constantly discharged to the load R. These energy transfers result in decreases in $i_{L\,k\,1}$ and $i_{L\,m}$ but

increases in $i_{L\,k\,2}$. This mode ends when current $i_{L\,k\,1}$ reaches zero at $t = t_3$

Mode IV $[t_3$, t_4]: During this interval, only magnetizing inductor L_m is constantly releasing its energy to C_2 . The current flow path is shown in Fig. 8(d), and only diode D_2 is conducting The iLm is decreasing due to the magnetizing inductor energy flowing through the coupled inductor $T1$ to secondary winding $N2$, and $D2$ continues to charge capacitor $C2$. The energy stored in capacitor $C3$ is constantly discharged to the load R. This mode ends when current iLm reaches zero at $t = t4$.

Mode V $[t4$, $t5$]: During this interval, all active components

are turned OFF; only the energy stored in capacitor $C3$ is continued to be discharged to the load R. The current flow path is shown in Fig. 8(e). This mode ends when switch $S1$ is turned ON at the beginning of the next switching period.
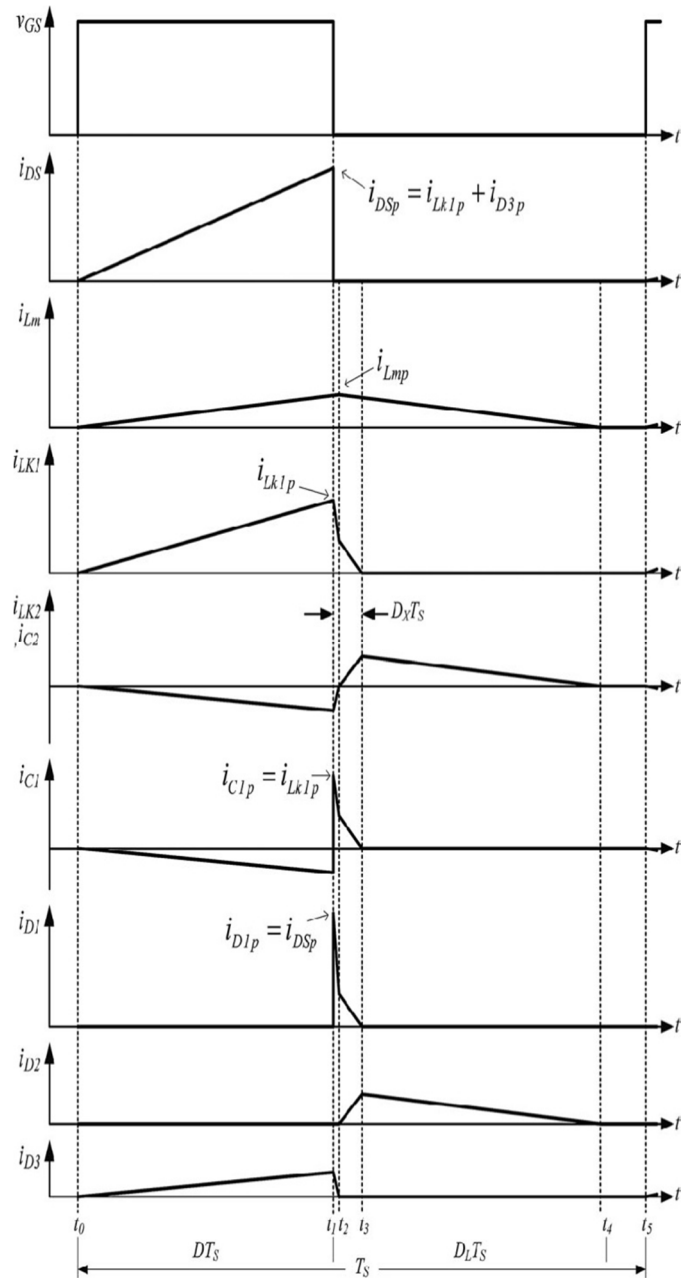

Fig. 6. Some typical waveforms of proposed converters at DCM operation
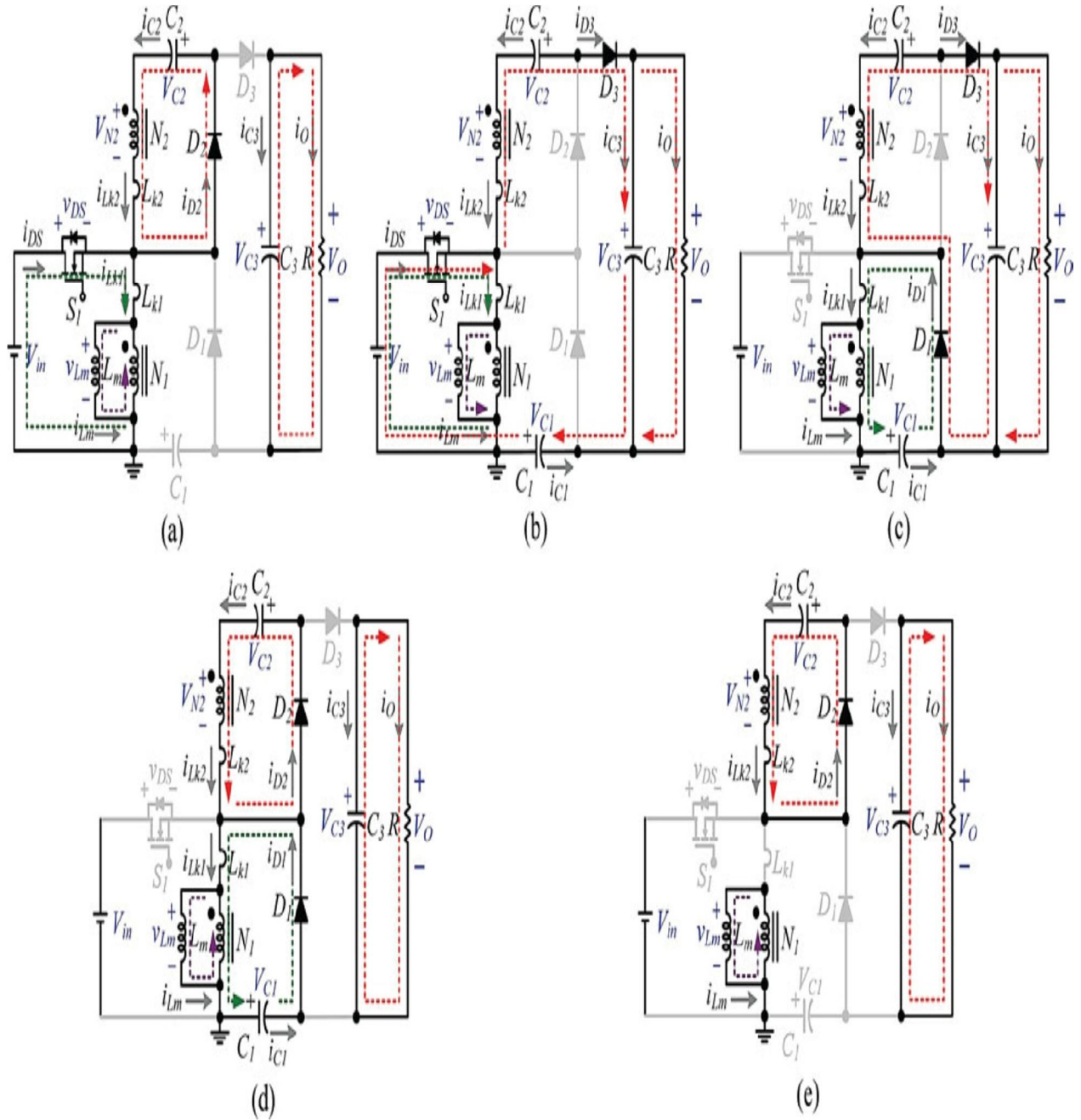
.

Fig. 7.Current flow path of five operating modes during.

(b) Mode II: $t_1 \sim t_2$. (c) Mode III: $t_2 \sim t_3$. (d) Mde IV: t_3

t_4 . (e) Mode V: $t_4 \sim t_5$.

IIISTEADY-STATE ANALYSIS OF PROPOSED CONVERTERS

A. CCM Operation

To simplify the steady-state analysis, only modes II and IV are considered for CCM operation, and the leakage inductances on the secondary and primary sides are neglected. The following equations can be written from Fig.7(b):
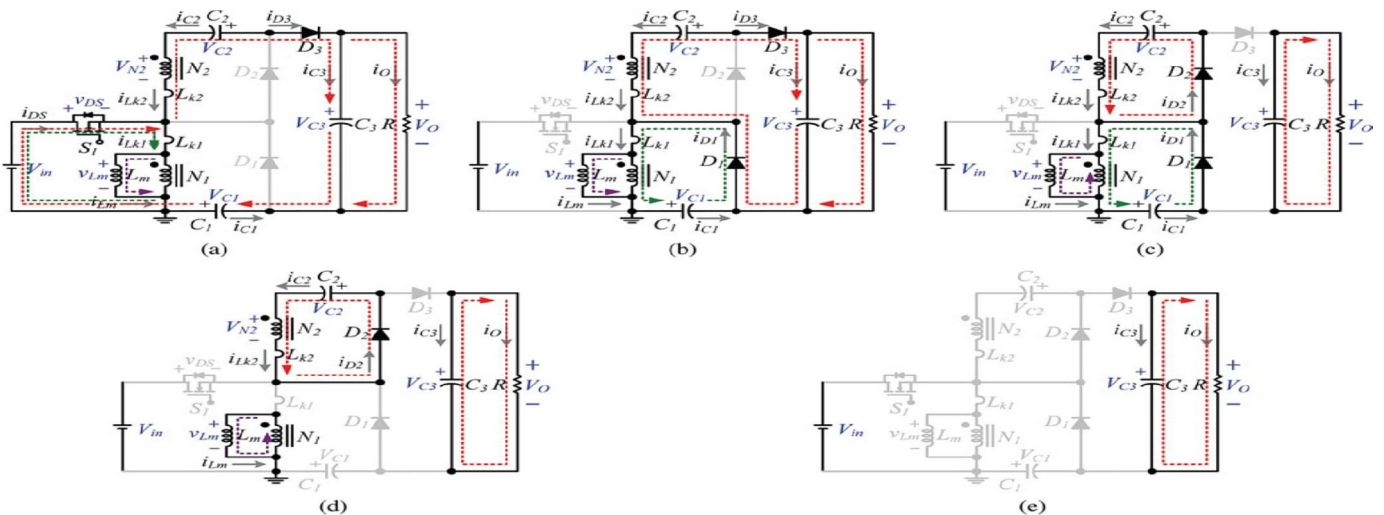
$$V = V \tag{1}$$

$$V = nV \tag{2}$$

During mode IV

$$V = -V \tag{3}$$

$$V = -V \tag{4}$$

Applying a volt-second balance on the magnetizing inductor Lm yields

$$(V)dt + (-V)dt \tag{5}$$

$$(nV)dt + (-V)dt \tag{6}$$

From which the voltage across capacitor C1 and C2 are obtained as follows:

$$V = \frac{D}{1-D} V \tag{7}$$

$$V = \frac{nD}{1-D} V \tag{8}$$

During mode II, the output $V_O = V_{in} + V_{N\,2} + V_{C\,2} + V_{C\,1}$ becomes

$$V = V + nV + \!\!-\!\!- V + \!\!-\!\!- V \tag{9}$$

The DC voltage gain Mccm can be found as follows:

$$Mccm = \!\!-\!\!- = \!\!-\!\!- \tag{10}$$

Both [10] and [11] are employing coupled inductor topology as the boost type converter integrating with coupled inductor ;this technology is similar to the technology of the proposed converter.fig shows the plot of voltage gain Mccm as function of the duty ratio D of the proposed converter is compared with that of available converters[10],[11].

The chart reveals the voltage gain Mccm of the proposed converters. All of them are operating under the same conditions:CCM and n=5.

one switching period at CCM operation (a) ModeI: $t_0 \sim t_1$.

Fig. 8. Current flow path of five operating modes during one Mode II: $t_1 \sim t_2$. (c) Mode III: $t_2 \sim t_3$. (d) Mode IV: $t_3 \sim t_4$.

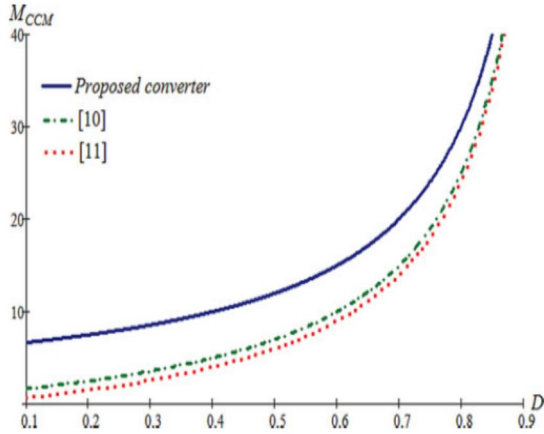
Fig 9 voltage gain as a function of the duty ratio of the proposed converter [10] and [11] under CCM operation and n=5.During CCM operation ,the voltage stresses on S1 and D1-D3 are given as

$$V \ = V \ = —— \tag{11}$$

$$V \ = —— \tag{12}$$

$$V \ = \frac{(\quad)}{\qquad} \tag{13}$$

From above equations values are calculated in ccm mode

switching period at DCM operation. (a) Mode I: $t_0 \sim t_1$.(b) (e) Mode V: $t_4 \sim t_5$.

B.DCM Operation

To simplify the steady-state analysis,only modes I and IV are considered for DCM operation ,and the leakage inductances on the secondary and primary sides are neglected. The following equations can be written from fig 8(b).when switch s1 is turned ON,the voltage levels across inductors Lm and secondary windingN2 are

$$V \ = V \tag{14}$$

$$V \ = nV \tag{15}$$

When switch s1 is turned OFF ,the voltage levels across inductors Lm and secondary winding N2 are

$$V \ = −V \tag{16}$$

$$V \ = −V \tag{17}$$

DL Ts is the period of time during which current iLm declines from peak current to zero.The voltage across Lm and secondary winding N2 can be found, as follows,by using the volt-second balance principle

$$(V \ )dt + \qquad (−V \ )dt \tag{18}$$

$$(nV \ )dt + \qquad (−V \ )dt \tag{19}$$

Which derives the voltage of C3,C4 and output voltage as

$$V \ = \frac{D}{DL} V \tag{20}$$

$$V \ = \frac{nD}{DL} V \tag{21}$$

$$V \ = \frac{(n + 1)(D + DL)}{DL} V \tag{22}$$

Equation (22) yielda DL as follows:

$$DL = \frac{(\quad)}{\underline{\quad}(\quad)} \qquad (23)$$

Since the average current of capacitor Ic1,Ic2 and Ic3 are zero in steady state ,the average current values for ID3,ID2 and ID1 are,respectively,equals to the average value of I0. The ILm is the peak current of the magnetizing inductor,as shown in the following:

$$ILmp = \underline{\quad} \qquad (24)$$

From fig 8(d) the average values for D1 and D2 are derived as

$$I0 = ID1 = \frac{(\quad)}{\underline{\qquad}} \qquad (25)$$

$$ID2 = \frac{(\qquad)}{\underline{\qquad}} \qquad (26)$$
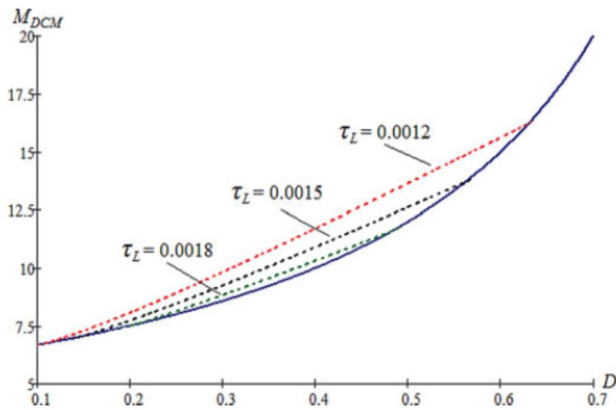

Fig. 10. Voltage gain as a function of the duty ratio of the propo[ ] under DCM operation with different τL by $n = 5$.

Since the average current values for $ID\,2$ and $ID\,1$ are, respectively,equal to the average value of IO (25) is equal to

(26),DX , which is defined as the duration during which diode current $iD\,1$ travels from peak down to zero, is

$$Dx = \frac{\quad}{(\quad)} \qquad (27)$$

Then, substituting (27) into (26), the IO can be rewritten as

$$I0 = \frac{\quad}{(\quad)} \qquad (28)$$

Since IO = VO / R, substituting (24) and (27) into (28) yields

$$\frac{\quad}{\underline{\quad}(\quad)} - D = \underline{\quad} \qquad (29)$$

The normalized magnetizing inductor time constant τL is defined as

$$TL = \underline{\quad} = \underline{\quad} \qquad (30)$$

where fS is the switching frequency. Substituting (30) into (29) obtains the voltage gain of the proposed converter in DCM, as follows:

$$MDCM = \underline{\quad} = \frac{(\quad)\overline{\quad}(\quad)(\quad)}{\underline{\qquad}} \qquad (31)$$

Equation (31) can be used to illustrate DCM voltage gain lines by different magnetizing inductor time constants τL, as shown in Fig. 10
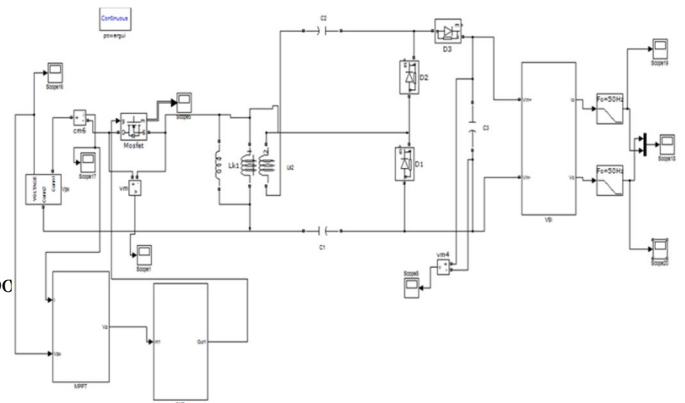The simulation diagram for the photovoltaic with MPPT is shown in fig 11.

Fig .11. Simulation diagram of solar with mppt

IV. EXPERIMENTAL RESULTS

A 100Wprototype sample is presented to verify the practicability of the proposed converter. The electrical specifications are $Vin = 15V$, $VO = 200V$, $fS = 50$ kHz, and full-load resistance $R = 400\ \Omega$. The major components required are $C1 = C2 = 47\ \mu F$ and $C3 = 220\ \mu F$. The main switch $S1$ is a MOSFET IXFK180N15P, the diodes $D1$ are MRB20200CTG, and the DPG30C300HB is selected for

$D2$ and $D3$. Since (10) assign turns ratio $n = 5$, the duty ratio D is derived as 55%.The boundary normalized magnetizing inductor time constant τLB is found by (28) to be 1.547×10^{-3} . To define the proposed converter's BCM operation at 50% of the full load, the load resistance $R = 800 \ \Omega$. The boundary magnetizing inductance LmB is found as follows:

$$\text{------} > 1.547 * 10$$

$$> 24.75 \mu H$$

The actual inductance of magnetizing inductor Lm of the coupled inductor is 30.54 μH, which is larger than boundary magnetizing inductance 24.75 μH. Fig. 11 shows voltage and current waveforms, which are measured from active switch $S1$, diodes $D1$, $D2$, and $D3$, and the current waveforms of $C1$ and $C2$ .The measured voltage spike across the active switch is found to be about 80V; this reveals that the energy of the leakage inductor has been stored in and voltage clamped by $C1$ These experimental waveforms agree with the operating principles and the steady-state analysis. Fig. 12 shows that the maximum efficiency of 95.3% occurred at 40% of full load; and the full-load efficiency is maintained at 92.3%. The efficiency variation is about 3%, and the flat efficiency curve is able to yield higher energy from the PV module during periods when sunlight is fading. The residential voltage discharge time of the proposed converter is 480 milliseconds, which prevents any potential electrical injuries to humans.The experimental output waveforms is shown in fig. 12 and fig. 13.
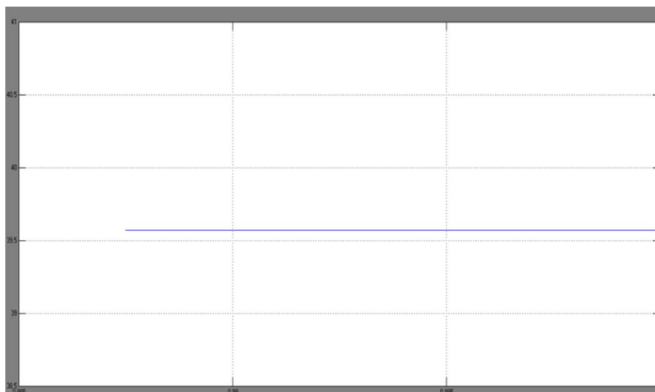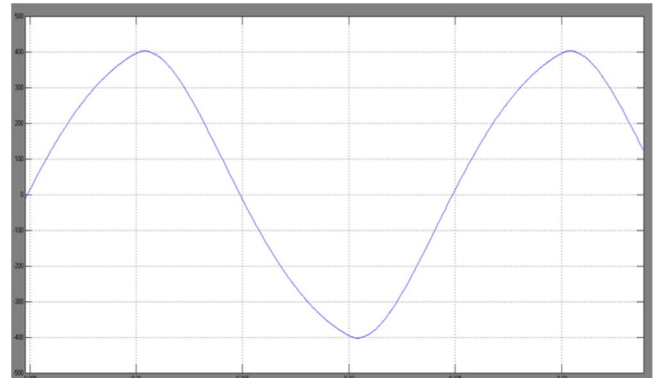

Fig 12. output from solar panel

Fig .13.voltage output .

V. CONCLUSION

Since the energy of the coupled inductor's leakage inductor has been recycled, the voltage stress across the active switch $S1$ is constrained, which means low ON-state resistance RDS(ON) can be selected. Thus, improvements to the efficiency of the proposed converter have been achieved. The switching signal action is performed well by the floating switch during system operation; on the other hand, the residential energy is effectively eliminated during the nonoperating condition, which improves safety to system technicians. From the prototype converter, the turns ratio $n = 5$ and the duty ratio D is 55%; thus, without extreme duty ratios and turns ratios, the proposed converter achieves high step-up voltage gain, of up to 13 times the level of input voltage. The experimental results show that the maximum efficiency of 95.3% is measured at half load, and a small efficiency variation will harvest more energy from the PV module during fading sunlight.

REFERENCES

[1] T. Shimizu,K.Wada, andN.Nakamura, "Flyback-type single-phase utility interactive inverter with power pulsation decoupling on the dc input for an ac photovoltaic module system," *IEEE Trans. Power Electron.*, vol. 21, no. 5,pp.1264–1272, Jan. 2006.
[2] C. Rodriguez and G. A. J. Amaratunga, "Long-lifetime power inverter for photovoltaic ac modules," *IEEE Trans. Ind. Electron.*, vol. 55, no. 7,pp. 2593–2601, Jul. 2008.
[3] S. B. Kjaer, J. K. Pedersen, and F. Blaabjerg, "A review of single-phase grid-connected inverters for photovoltaic modules," *IEEE Trans. Ind. Appl.*, vol. 41, no. 5, pp. 1292–1306, Sep./Oct. 2005.
[4] J. J. Bzura, "The ac module: An overview and update on self-contained modular PV systems," in *Proc. IEEE Power Eng. Soc. Gen. Meeting*, Jul. 2010, pp. 1–3.

[5] B. Jablonska, A. L. Kooijman-van Dijk, H. F. Kaan, M. van Leeuwen, G. T. M. de Boer, and H. H. C. de Moor, "PV-PRIV′E project at ECN, five years of experience with small-scale ac module PV systems," in *Proc. 20th Eur. Photovoltaic Solar Energy Conf.*, Barcelona, Spain, Jun. 2005,pp. 2728–2731.

[6] T. Umeno, K. Takahashi, F. Ueno, T. Inoue, and I. Oota, "A new approach to lowripple-noise switching converters on the basis of switched- capacitor converters," in *Proc. IEEE Int. Symp. Circuits Syst.*, Jun. 1991, pp. 1077–1080.

[7] B. Axelrod, Y. Berkovich, and A. Ioinovici, "Switched-capacitor/ switched-inductor structures for getting transformerless hybrid dc–dc PWM converters," *IEEE Trans. Circuits Syst. I, Reg. Papers*, vol. 55,no. 2, pp. 687–696, Mar. 2008.

[8]Seok-Il Go, Seon-Ju Ahn, Joon-Ho Choi†, Won-Wook Jung, Sang-Yun Yun and Il-Keun Song," Simulation and Analysis of Existing MPPT Control Methods in a PV Generation System " in proc. *Journal of International Council on Electrical Engineering Vol. 1, No. 4, pp. 446~451, 2011.*

[9] H. Chung and Y. K. Mok, "Development of a switched-capacitor dc–dcboost converter with continuous input current waveform," *IEEE Trans.Circuits Syst. I, Fundam. Theory Appl.*, vol. 46, no. 6, pp. 756–759, Jun.1999.

[10] T. J. Liang and K. C. Tseng, "Analysis of integrated boost-flyback step-up converter," *IEE Proc. Electrical Power Appl.*, vol. 152, no. 2, pp. 217–225,Mar. 2005.

[11] Q. Zhao and F. C. Lee, "High-efficiency, high step-up dc–dc converters,"*IEEE Trans. Power Electron.*, vol. 18, no. 1, pp. 65–73, Jan. 2003.

[12] M. Zhu and F. L. Luo, "Voltage-lift-type cuk converters: Topology and analysis," *IET Power Electron.*, vol. 2, no. 2, pp. 178–191, Mar.2009.

[13] J. W. Baek, M. H. Ryoo, T. J. Kim, D. W. Yoo, and J. S. Kim, "High boost converter using voltage multiplier," in *Proc. IEEE Ind. Electron. Soc. Conf. (IECON)*, 2005, pp. 567–572.

[14] J. Xu, "Modeling and analysis of switching dc–dc converter with coupledinductor,"in *Proc. IEEE 1991 Int. Conf. Circuits Syst. (CICCAS)*, 1991,pp. 717–720.

[15] R. J.Wai, C. Y. Lin, R. Y. Duan, and Y. R. Chang, "High-efficiency dc–dcconverter with high voltage gain and reduced switch stress," *IEEE Trans.Ind. Electron.*, vol. 54, no. 1, pp. 354–364, Feb. 2007.

[16] S. M. Chen, T. J. Liang, L. S. Yang, and J. F. Chen, "A cascaded high step-up dc–dc converter with single switch for microsource applications,"*IEEE Trans. Power Electron.*, vol. 26, no. 4, pp. 1146–1153, Apr. 2011.

[17] T. J. Liang, S. M. Chen,L. S.Yang, J. F. Chen, and A. Ioinovici, "Ultra large gain step-up switched-capacitor dc–

dc converter with coupled inductor for alternative sources of energy," *IEEE Trans. Circuits Syst. I*, to be published.

[18] L. S. Yang and T. J. Liang, "Analysis and implementation of a novel bidirectional dc–dc converter," *IEEE Trans. Ind. Electron.*, vol. 59, no. 1, pp. 422–434, Jan. 2012.

[19] W. Li and X. He, "Review of non-isolated high-step-up dc/dc converters in photovoltaic grid-connected applications," *IEEE Trans. Ind. Electron.*, vol. 58, no. 4, pp. 1239–1250, Apr. 2011.

[20] S. H. Park, S. R. Park, J. S. Yu, Y. C. Jung, and C. Y. Won, "Analysis and design of a soft-switching boost converter with an HI-Bridge auxiliary resonant circuit," *IEEE Trans. Power Electron.*, vol. 25, no. 8, pp. 2142–2149, Aug. 2010.

[21] G. Yao, A. Chen, and X. He, "Soft switching circuit for interleaved boost converters," *IEEE Trans. Power Electron.*, vol. 22, no. 1, pp. 80–86, Jan. 2007.

[22] Y. Park, S. Choi,W. Choi, and K. B. Lee, "Soft-switched interleaved boost converters for high step-up and high power applications," *IEEE Trans.Power Electron.*, vol. 26, no. 10, pp. 2906–2914, Oct. 2011.

[23] Y. Zhao, W. Li, Y. Deng, and X. He, "Analysis, design, and experimentation
of an isolated ZVT boost converter with coupled inductors," *IEEE Trans. Power Electron.*, vol. 26, no. 2, pp. 541–550, Feb. 2011.

[24] H. Mao, O. Abdel Rahman, and I. Batarseh, "Zero-voltage-switching dc–dc converters with synchronous rectifiers," *IEEE Trans. Power Electron.*,
vol. 23, no. 1, pp. 369–378, Jan. 2008.

[25] J. M. Kwon and B. H. Kwon, "High step-up active-clamp converter with input-current doubler and output-voltage doubler for fuel cell power systems,"*IEEE Trans. Power Electron.*, vol. 24, no. 1, p. 108–115, Jan. 2009.

[26] S. Dwari and L. Parsa, "An efficient high-step-up interleaved dc–dc converter with a commonactive clamp," *IEEE Trans.Power Electron.*, vol. 26, no. 1, pp. 66–78, Jan. 2011.

[27] C. Restrepo, J. Calvente, A. Cid, A. El Aroudi, and R. Giral, "A noninverting buck-boost dc–dc switching converter with high efficiency and wide bandwidth," *IEEE Trans. Power Electron.*, vol. 26, no. 9, pp. 2490–2503, Sep. 2011.

[28] K. B. Park, G.W.Moon, and M. J. Youn, "Nonisolated high step-up boost converter integrated with sepic converter," *IEEE Trans. Power Electron.*,vol. 25, no. 9, pp. 2266–2275, Sep. 2010.

[29] L. S. Yang, T. J. Liang, and J. F. Chen, "Transformerless dc–dc converters with high step-up voltage gain," *IEEE Trans. Ind. Electron.*, vol. 56, no. 8,pp. 3144–3152, Aug. 2009.

[30] N. Pogaku, M. Prodanovic, and T. C. Green, "Modeling, analysis and testing of autonomous operation of an inverter-based microgrid," *IEEE Trans. Power Electron.*, vol. 22, no. 2, pp. 613–625, Mar. 2007.

[31] B. Axelrod, Y. Berkovich, and A. Ioinovici, "Transformerless dc–dc converters with a very high dc line-to-load voltage ratio," in *Proc. IEEE Int. Symp. Circuits Syst. (ISCAS)*, 2003, vol. 3, pp. 435–438.